Chitin and Chitosan Nanocomposites for Tissue Engineering

Arun Kumar Mahanta and Pralay Maiti

Abstract Chitin and chitosan are the most widely used biodegradable and biocompatible materials subsequent to cellulose. Nowadays a wide range of materials, including those classified as organic, inorganic, and biological are used in the synthesis, fabrication, and processing of nanostructures with unique physical properties. The properties of the polymer significantly improve by dispersing a few percentage of nanoparticle in the polymer matrix. In this context, we are focusing on the preparation, characterization, and bioactivity of chitin and chitosan nanocomposite in detail. The morphological changes occur in presence of nanoparticle. The improvement of thermal and mechanical properties including dynamic mechanical behavior of chitin and chitosan in presence of different nanofillers has been discussed in detail with suitable example as potential material for bone and wound tissue engineering applications. We summarize the physicochemical and drug delivery properties of chitin and chitosan composites. The cytocompatibility of the nanocomposites is assessed with improved cell attachment and proliferation using different human cells. This chapter enhances the understanding of biological uses of chitin and chitosan with their improved properties in presence of nanoparticles. A new approach at the intersection of biology and nanotechnology is focused to develop the next promising eco-friendly biopolymer nanocomposites.

Keywords Chitin/chitosan · Nanoparticle · Biomaterial · Drug delivery

1 Introduction

In recent years, tissue engineering has been widely investigated as a promising approach toward regeneration of tissue [1]. Biomaterials are required in tissue engineering strategies for the cell growth, attachment, and proliferation [2, 3].

A.K. Mahanta · P. Maiti (✉)
School of Materials Science and Technology, Indian Institute of Technology (Banaras Hindu University), Varanasi 221005, India
e-mail: pmaiti.mst@itbhu.ac.in

P.K. Dutta (ed.), *Chitin and Chitosan for Regenerative Medicine*, Springer Series on Polymer and Composite Materials, DOI 10.1007/978-81-322-2511-9_6

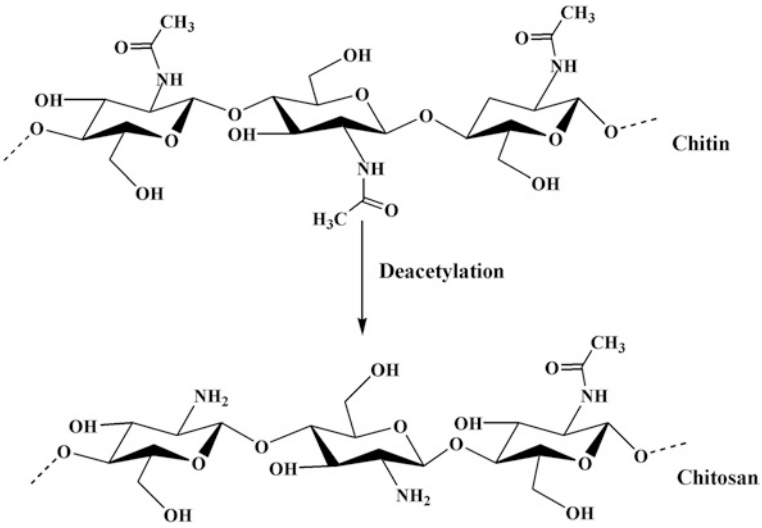

Fig. 1 Chemical structure of chitin and deacetylated chitin (chitosan)

Polysaccharides have the tendency to be extremely bioactive and classified as natural macromolecules. These polysaccharides are generally derived using different biotechnological approaches from agricultural feed stock or crustacean shell waste. In terms of availability, chitin is the second most abundant polymer after cellulose. Chitosan, a deacetylated derivative of chitin has multidirectional application such as in food and nutrition, material science, biotechnology, pharmaceuticals, agricultural and environmental protection [4–9]. Chitin contains two monomeric units D-glucosamine and *N*-acetyl-D-glucosamine which are interconnected by β-glycosidic linkages [10]. It is found in nature as ordered crystalline microfibrils forming structural components in the exoskeleton of arthropods or in the cell walls of fungi and yeast [11]. Chitosan is the most important derivative of chitin, obtained by (partial) deacetylation of chitin in the solid state under alkaline condition (concentrated NaOH) or by enzymatic hydrolysis in the presence of chitin deacetylase [12, 13]. The structure of chitin and chitosan is presented in Fig. 1. Chitin exists in three different polymorphic forms, with varying properties and the different forms are α, β, and γ [14–17]. The sources of α-chitin are crabs and shrimps; β-chitin is squids; and γ-chitin is loligo. The different polymorphic forms differ in their arrangement of polymeric chains like, antiparallel conformation to each other in α-chitin, polymeric chains are arranged in parallel configuration in β-chitin, and polymeric chains are arranged in two parallel chains followed by one antiparallel chain in γ-chitin [17]. Chitin and chitosan are biocompatible, biodegradable, and nontoxic [18–21] and they offer the advantage of being easily processed into gels [22], membranes [23, 24], nanofibers [25], nanofibrils [26], beads [27], microparticles [28], nanoparticles [29, 30], scaffolds [31–33], and sponge-like forms [34]. Owing to their special character and easily

processable nature, chitin and chitosan have versatile applications in tissue engineering [34–42], wound healing [43–50], drug delivery [51–56], and gene delivery [57]. Nowadays, nanocomposite of biopolymers and bioactive materials has been extensively used in tissue engineering [58]. The aim of making nanocomposite is achieving a better interaction between the bioactive inorganic phase and the organic phase to get considerably enhanced properties. Nanometer size or nanostructure materials known as nanomaterials, where at least one dimension is in the nanometer scale, are the backbone of nanoscience and nanotechnology. They have unique physicochemical properties compared with the bulk materials of the same composition and capable of changing their properties and applications. Nanomaterials are mostly found as: (1) carbon-based material, consists of carbon atoms and possesses different nanostructures, e.g., single-wall or multiwall carbon nanotubes (CNT), graphene, and fullerene; (2) metallic nanomaterials which is composed of nanomaterials of metals, transition metals or their compounds and composites, e.g., gold, iron oxide, silver, silica, and quantum dots; (3) silicon nanomaterials which consist of silicon or its compound, e.g., silicon or silica nanoparticles and (4) organic nanomaterials, formed via agglomeration or assembly of organic molecules, e.g., dendrimers, polymers biomolecules, or biomacromolecules [59]. Chitin and chitosan both contain hydroxyl groups at C-3 and C-6 positions and in addition to that chitosan contains some extent of amino groups at C-2 position depending on the degree of deacetylation, therefore, they can interact with the nanomaterials through various means. There have been several reports on preparations and applications of chitin and chitosan nanocomposites. In this chapter, an attempt has been made to focus on the application potential on chitin and chitosan-based nanocomposites with different filler nanomaterials for tissue engineering, drug delivery, and antimicrobial activities.

2 Composites Preparation

There are several processes to prepare nanocomposites with the advantages or drawbacks. Some common processes which are frequently used to prepare the chitin and chitosan nanocomposites are illustrated as follows:

(a) *Solution casting method* This is the simplest technique to prepare polymer nanocomposites. In this technique, three steps are required to prepare the nanocomposites. At first, the filler is dispersed/dissolved in the appropriate solvent through mechanical stirring or sonication. The required polymer is dissolved in the same solvent or in two miscible solvents. Finally, the filler solution and polymer solution are mixed together at room temperature or other suitable temperatures. Composites are obtained either by precipitation or casting the solution mixture. Regiel-Futyra et al. have prepared chitosan–gold nanocomposite film through solution casting method [60]. They have poured the chitosan-based gold nanoparticles dispersion into Petri dishes and dried in an air oven at 60 °C until the solvent was evaporated completely.

(b) *In situ technique* This is the most efficient technique to prepare the composites with uniformly distributed filler materials. Filler materials are dispersed in monomer either in presence or absence of solvent followed by the addition of curing agents or the hardener for polymerization at experimental temperature. The major advantage of this technique is that the composites are obtained with improved properties. Sometimes nanomaterials are synthesized in reaction mixture at the same reaction condition. Hebeish et al. prepared chitosan-grafted-poly acrylonitrile silver nanocomposites via in situ chemical reduction of Ag ions in graft copolymerisation of acrylonitrile on to chitosan [61].

(c) *Electro spinning technique* There are three major components in electrospinning instruments: a high-voltage power supply, a spinneret (a metallic needle), and a collector (a grounded conductor). The spinneret is connected to a syringe in which the mixture of polymer and nanomaterial solution is hosted. When high voltage (usually in the range of 1–30 kV), is applied, the pendent drop of solution at the nozzle of spinneret will become highly electrified and the induced charges are evenly distributed over the surface. When a sufficiently high voltage is applied the electrostatic repulsion counteracts the surface tension and the droplet is stretched. Such type of electrified jet then undergoes a stretching and whipping process, leading to the formation of long and thin thread. The threads are collected by the grounded collector placed under the spinneret. With the use of this relatively simple and straightforward technique several polymer composites have been processed as fibers with diameters ranging from tens of nanometers to a few micrometers. Naseri et al. developed electrospun chitosan/polyethylene oxide-based randomly oriented fiber mats reinforced with chitin nanocrystals using electrospinning technique [62].

(d) *Freeze–drying technique* This is another method to fabricate polymer composite scaffolds with variable porosity and pore size and utilizes emulsion/freeze–drying process. The homogenized mixture of polymer and filler solution is poured into copper mold and quenched in liquid nitrogen or in required lower temperature. After quenching, the polymer scaffold is freeze–dried to remove the solvents. The obtained scaffolds have the porosity up to 90 % and median pore sizes in the range of 15–35 μm with an interconnected pore structure. In comparison to solvent casting, the scaffolds offer much higher specific pore surface area as well as the ability to make thick (>1 cm) polymer scaffolds. Such types of scaffolds have drawn very much attention in tissue engineering. Liu et al. have developed novel chitosan–halloysite nanotubes (HNTs) nanocomposite (NC) scaffolds by combining solution-mixing and freeze–drying techniques [63].

3 Dispersion of Nanoparticles

The properties of nanocomposites depend on the extent of dispersion of nanoparticles in polymer matrices. The dispersion can be evaluated through electron microscope; transmission electron microscope (TEM), Scanning Electron

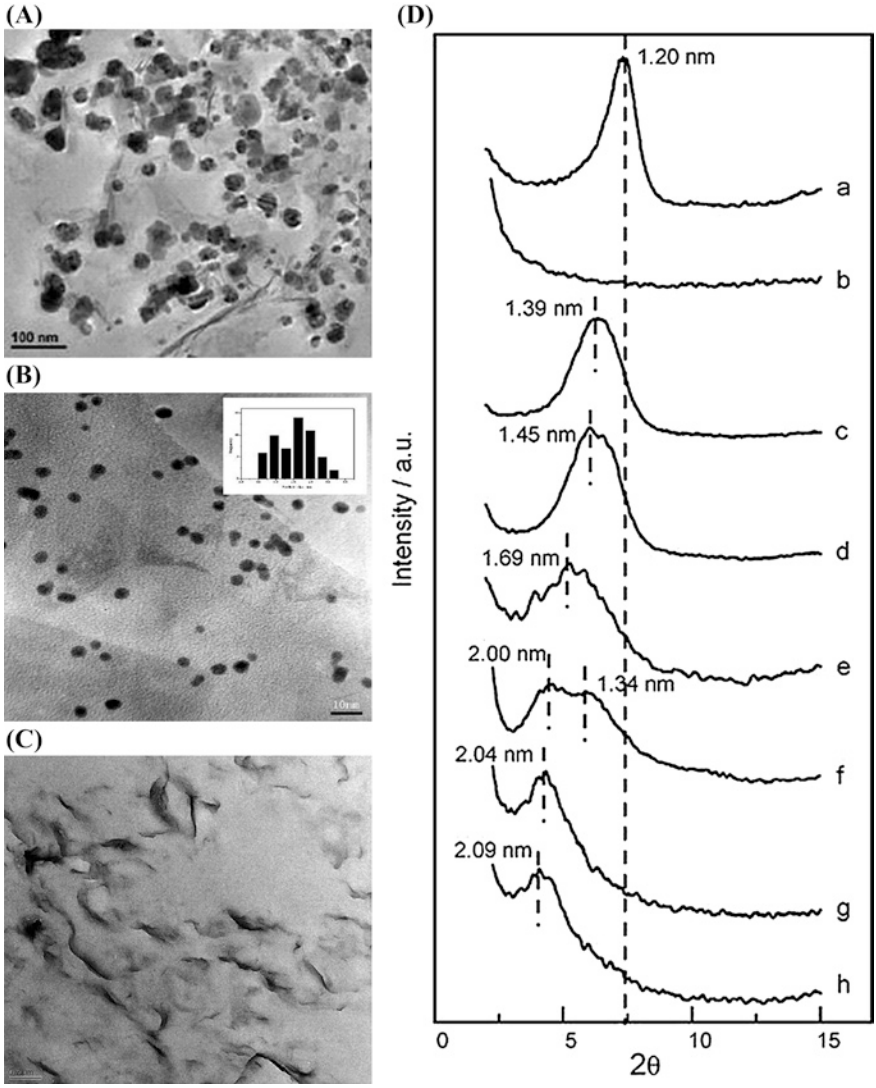

Fig. 2 TEM image of **A** Ag–Fe_3O_4/chitosan nanocomposite, [64] **B** gold/chitosan nanocomposite, [65] and **C** montmorillonite/chitosan nanocomposite, [66] and **D** XRD patterns of **a** Na^+-montmorillonite, **b** chitosan film, and nanocomposites prepared from chitosan–clay ratios of **c** 0.25:1, **d** 0.5:1, **e** 1:1, **f** 2:1, **g** 5:1, and **h** 10:1 [67]

Microscope (SEM), or Atomic Force Microscopy(AFM). The Ag–Fe_3O_4 nanoparticles with spherical shapes having mean diameters of 10–40 nm are dispersed uniformly in the chitin matrix in Fig. 2a [64]. Figure 2b shows the typical TEM image of gold nanoparticle in chitosan–gold nanocomposites showing the histogram of particle size distribution [65]. The image (Fig. 2b)

displays monodisperse gold nanoparticles, which are homogeneously distributed in the nanocomposite. The particles are found to be spherical with a narrow size distribution; the average particle diameter is about 4 nm. Gold nanoparticles are found to have a very stable state as no aggregation of gold particles is observed in TEM after 2 months. Wang et al. reported that with the lower content (2.5 wt%) of montmorillonite (MMT) the chitosan–MMT nanocomposite shows the coexistence of both intercalated and exfoliated structures [66]. With the increase in content of MMT (5 wt%) intercalated with occasional flocculation morphology is observed (Fig. 2c). The formation of flocculated structure in chitosan/MMT nanocomposite with higher content of MMT is due to the hydroxylated edge–edge interaction of the silicate layers. The strong interaction between chitosan and MMT through the amino and hydroxyl groups of chitosan with the silicate hydroxylated edge groups, is believed to be the main driving force for the good dispersion of MMT in chitosan matrix to form flocculated structure.

The cationic biopolymer chitosan was intercalated in Na^+-montmorillonite to get compact and robust three-dimensional nanocomposites with interesting functional properties [67]. Figure 2d shows the XRD pattern of clay, chitosan, and chitosan–clay composites. The intercalation of chitosan in clay gallery is confirmed by the decrease of 2θ values with the increase of chitosan–clay ratio.

4 Morphology

The morphology of the nanocomposite is investigated using SEM, AFM, and optical microscope. Figure 3a represents the cross-sectional structure of pure chitosan and the chitosan–halloysite nanotubes (HNTs) nanocomposite scaffolds prepared by freeze–drying technique [63]. Both pure chitosan and its nanocomposites display a highly porous, open, and 3D interconnected morphology with the pore size around 200 μm. The chitosan–HNTs nanocomposite scaffolds show more uniform porous structure and less collapse of the pore walls than chitosan which may be attributed to the enhanced pore forming ability of chitosan by HNTs due to the strong interaction. In addition to that, nanocomposite scaffolds with HNTs have slightly larger pore size than that of pure chitosan scaffolds. The interaction between chitosan and HNTs causes absorption of chitosan on the surface of HNTs. It is clear from Fig. 3b (a) that HNTs have cylindrical-shaped tubular morphology and open-ended lumen along the nanotubes. The edge of HNTs is clear and sharp while the edge of chitosan–HNTs is obscure and blurred (Fig. 3b (b)). The SEM image of chitin and chitin–HNTs is shown in Fig. 3c [68]. Both chitin and chitin–HNTs hydrogel display large interconnected pores with pore size of 100–200 μm. The average pore size of chitin and chitin–HNTs hybrid hydrogel with low HNTs concentration are about 200 μm, while the pore walls are found in several micrometers. The hybrid hydrogel exhibits reduced pore size with

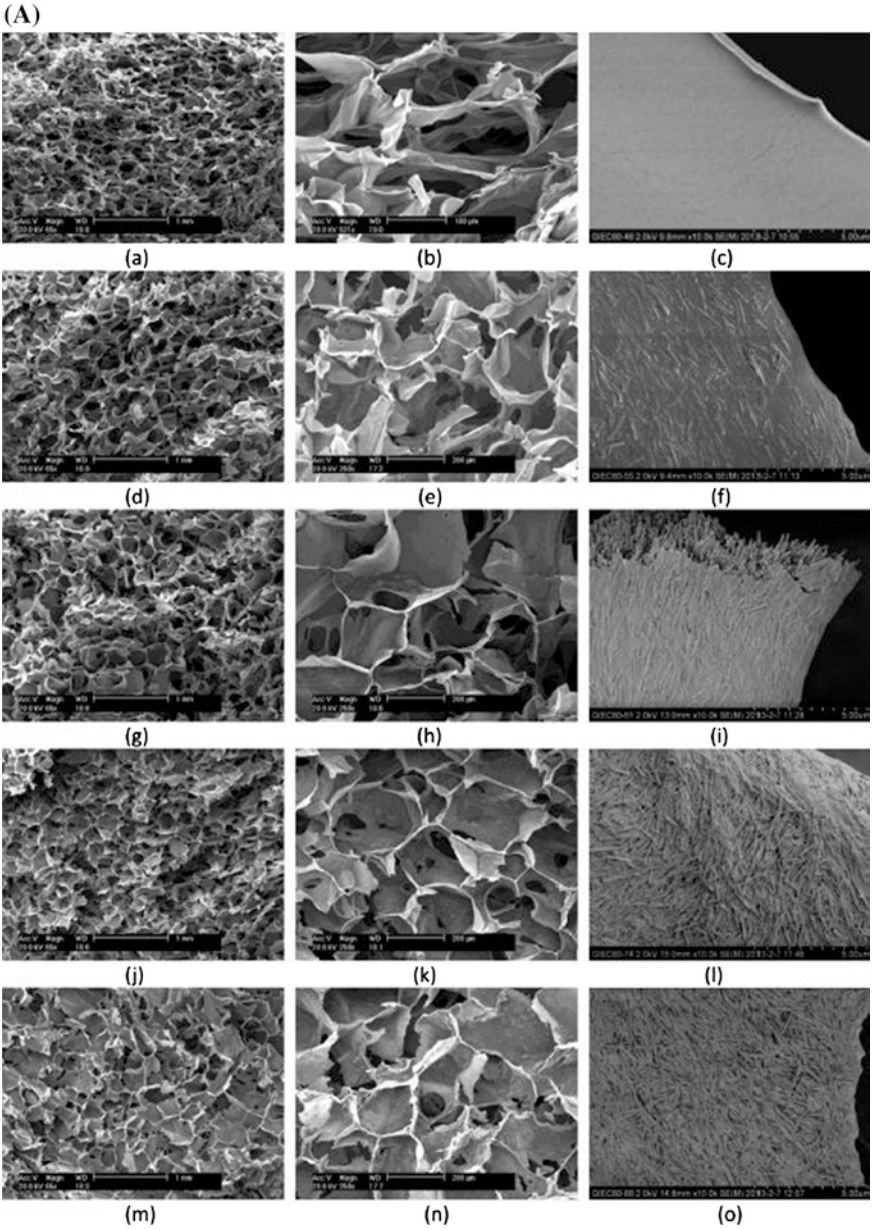

Fig. 3 **A** SEM micrographs of freeze–dried chitosan and chitosan–HNTs NC scaffolds with different magnifications: pure chitosan (**a**–**c**); CS2N1 (**d**–**f**); CS1N1 (**g**–**i**); CS1N2 (**j**–**l**); and CS1N4 (**m**–**o**). [63] **B** AFM images of HNTs and chitosan–HNTs (50 wt% HNTs): (**a** and **c**) HNTs; (**b** and **d**) chitosan–HNTs. The samples were prepared by dipping the dilute HNTs and chitosan–HNTs aqueous dispersions on freshly clean mica, [63] and **C** SEM photos for freeze–dried chitin and chitin–HNTs hybrid hydrogels: **a** chitin; **b** CT2N1; **c** CT1N1; **d** CT1N2; **e** CT1N4 [68]

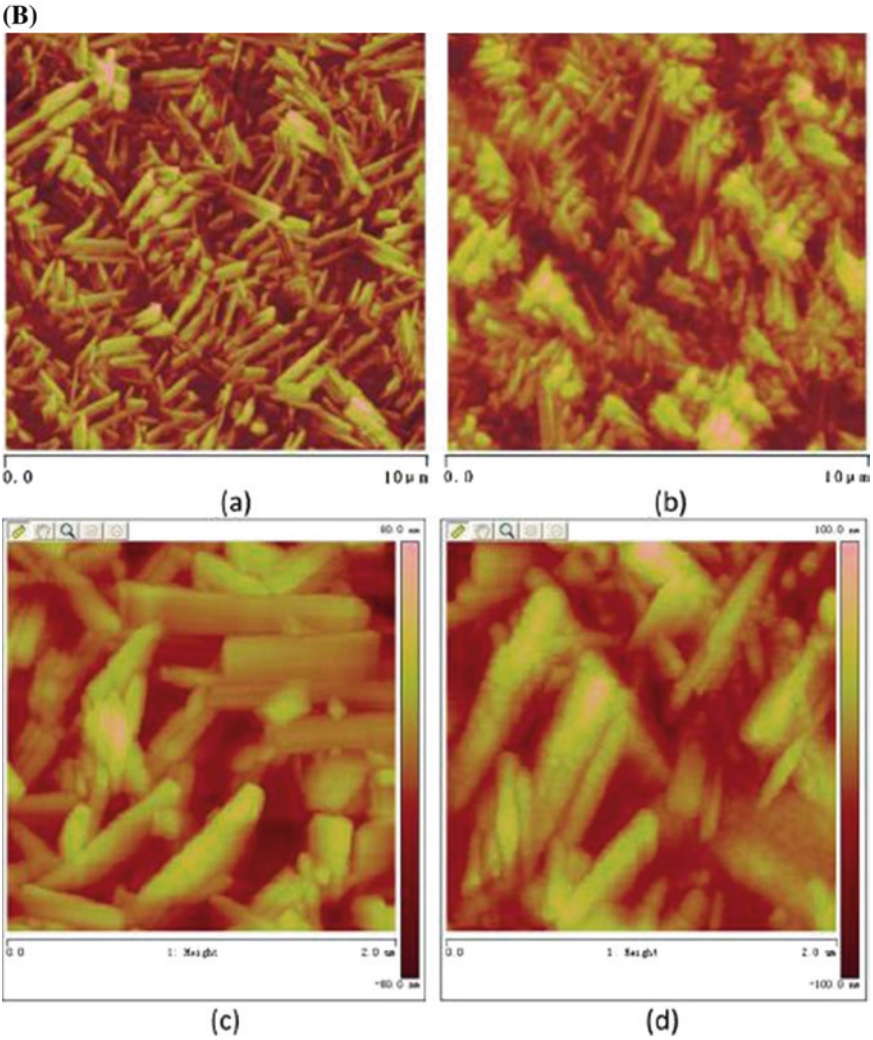

Fig. 3 (continued)

high HNTs concentration (CT1N4) as a result of the decrease in water volume in hydrogel. Kumar et al. reported that β-chitin hydrogel/nanohydroxyapatite (nHAp) nanocomposite scaffolds prepared by freeze–drying are porous in nature [69]. They have found that the porosity of the scaffolds is decreased with the increase in the concentration of nHAp. The nHAp particles intact the polymer chain acting as filler and hence cause a reduction in the porosity. In the case of control, the pores were arranged uniformly and interconnected with wall.

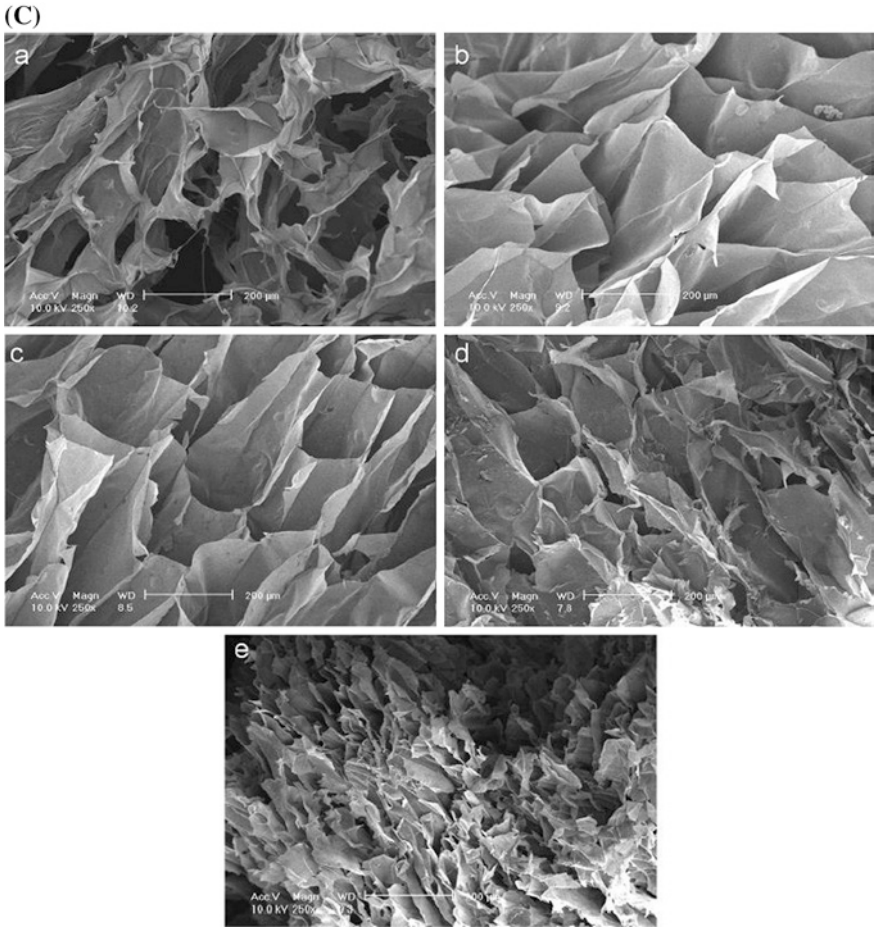

Fig. 3 (continued)

5 Thermal Properties

Thermal stability of nanocomposite is assessed from the weight loss as a function of time. Novel chitosan–halloysite nanotubes (HNTs) nanocomposites (NC) scaffolds were developed by Liu et al. [63]. They have reported that the interaction between HNTs and chitosan can affect the thermal stability of chitosan scaffolds. Figure 4 shows the TGA and DTG curves of chitosan and chitosan–HNTs nanocomposites scaffolds. Three stages of decomposition of chitosan at around 70, 163, and 273 °C are observed, which are related to the loss of free water, loss of bonded water, and the degradation of the chitosan chains, respectively, whereas HNTs show only one peak at 483 °C due to the structural dehydroxylation of HNTs. Chitosan–HNTs nanocomposites show only two peaks which are

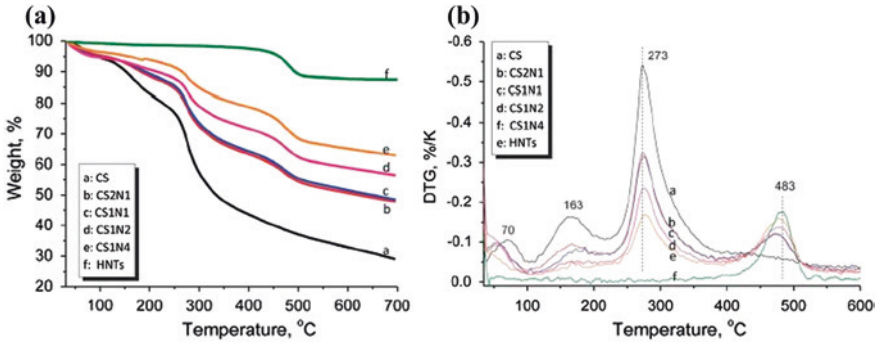

Fig. 4 TGA (**a**) and DTG (**b**) curves for CS, HNTs, and CS–HNTs NC scaffolds [63]

assigned to the degradation of chitosan and HNTs, respectively. It is observed from the DTG curves that the degradation temperature of chitosan component is slightly increased as compared to pure chitosan while the degradation temperature of HNTs component is slightly decreased as compared to pristine HNTs. The degradation temperature of chitosan and HNTs components are 277 and 477 °C in composites where weight ratio of chitosan (CS) and HNTs (N) was 1:4. These degradation temperatures are 4 °C higher and 6 °C lower than pure chitosan and pristine HNTs, respectively. Chitosan–montmorillonite nanocomposites prepared through anion exchange method between water-soluble oligomeric chitosan and a Na^+-montmorillonite shows higher thermal stability than pure chitosan [70]. This thermal resistance arises from the electrostatic interaction between chitosan and silicate layer. Chitosan–hyaluronan (HYA)/nano-chondrotin sulfate (nCS) composites show lower thermal stability than neat chitosan but high temperature resistance than chitosan–HYA [71]. Marroquin et al. reported the thermal degradation of 5 % MWNT/chitosan and 5 % Fe_3O_4/MWNT/chitosan nanocomposite [72]. They observed three major peaks in DTG curves. The first peak around 50–120 °C is associated with the evaporation of physically absorbed and strongly hydrogen-bonded water to chitosan and MWNT. 46 % drop in weight of nanocomposite was observed at around 120–400 °C range. This was associated with depolymerization of chitosan chains through deacetylation and cleavage of glycosidic linkages via dehydration and deamination. The thermal destruction of the pyranose ring produce formic, acetic, and butyric acids as well as a series of lower fatty acids at 400–700 °C. Additional third stage degradation suggested at 750–800 °C corresponds to the reduction of Fe_3O_4 by the reaction with residual carbon. The overall higher thermal stability of Fe_3O_4 containing nanocomposite is due to the incorporation of these nanoparticles into the chitosan matrix which affects the activation energy of the first and major stage of decomposition and also suggests a hindrance of depolymerisation of the main chitosan chains through chemical interactions. Chitosan membranes reinforced by halloysite nanotubes (HNTs) in the concentration range of 2–15 (w/w%) have been prepared by solution casting which shows

a drastic enhancement of thermal stability with increasing HNTs concentration in the composite [73]. Enhancement of this thermal stability might be due to two main reasons. The char residue of chitosan/HNTs composite may act as a barrier, therefore, lead to effective delay in heat transport and hinder the volatile escape while help improving the thermal stability. Chitosan/HNTs shows significant thermal stability at higher concentration by adding 15 (w/w%) HNTs into the chitosan matrix. Cellulose nanocrystals (CNCs) enhance the thermal resistance of poly (vinyl alcohol)/chitosan (PVA/CS) bio-nanocomposites films [74]. PVA/CS/CNCs bio-nanocomposite with the 0.5 and 1.0 wt% CNCs show thermal degradation at 288 and 337 °C, respectively. The interactions between the abundant hydroxyl groups of CNCs and the free hydroxyl groups of PVA/CS through hydrogen bonding are key for increasing thermal stability of PVA/CS/CNCs bio-nanocomposite. It is observed that a relatively higher concentration of CNCs like 3 and 5 wt% show degradation at lower temperature at 322 and 311 °C. The decrease in degradation temperature might be due to heterogeneous size distribution and aggregation of nanocrystals within the polymer matrix. Jayakumar et al. reported that with the incorporation of nano-TiO_2 particle into the chitin–chitosan matrix make the chitin–chitosan/nano-TiO_2 composite scaffolds more thermally stable than the control chitin–chitosan scaffolds [75].

6 Mechanical Properties

Wang et al. have prepared nanocomposite of chitosan with the functionalized multiwalled carbon nanotubes (MWCNTs) with different wt% of MWCNTs loading in chitosan matrix [76]. The MWCNTs were functionalized to increase the carboxylic and hydroxyl groups through refluxing in a mixture of concentrated sulphuric acid and nitric acid. They have measured the mechanical properties through uniaxial extension. The typical stress–strain curves (Fig. 5a) showed that tensile modulus and tensile strength of the composite increase about 78 and 94 % with 0.4 wt% loading of MWCTs filler where as it increased to about 93 and 99 %, respectively, with the 0.8 wt% of filler. The increase of mechanical properties of chitosan/MWCNTs nanocomposite as compared to those neat chitosan is due to (a) the reinforcement effect of finely dispersed high-performance MWCNTs nanofillers throughout the chitosan matrix, and, (b) strong interaction of MWCNTs with the chitosan through carboxylic and hydroxyl groups of functionalized MWCNTs with the amino, primary, and secondary hydroxyl groups of chitosan. Yang et al. prepared chitosan/graphene oxide nanocomposite (CS/GO) [77]. The obtained mechanical properties (Fig. 5b) in uniaxial extension indicate that with an increase in GO loading from 0 to 1 wt% not only increase the strength but also elongation at break than those of pure CS. The crystallinity of the chitosan is changed with the addition of GO which is an important factor for the enhancement of tensile properties of the polymers. Casariego et al. showed the higher tensile strength of chitosan–micro/nanoclay (MNC) particle composite films with

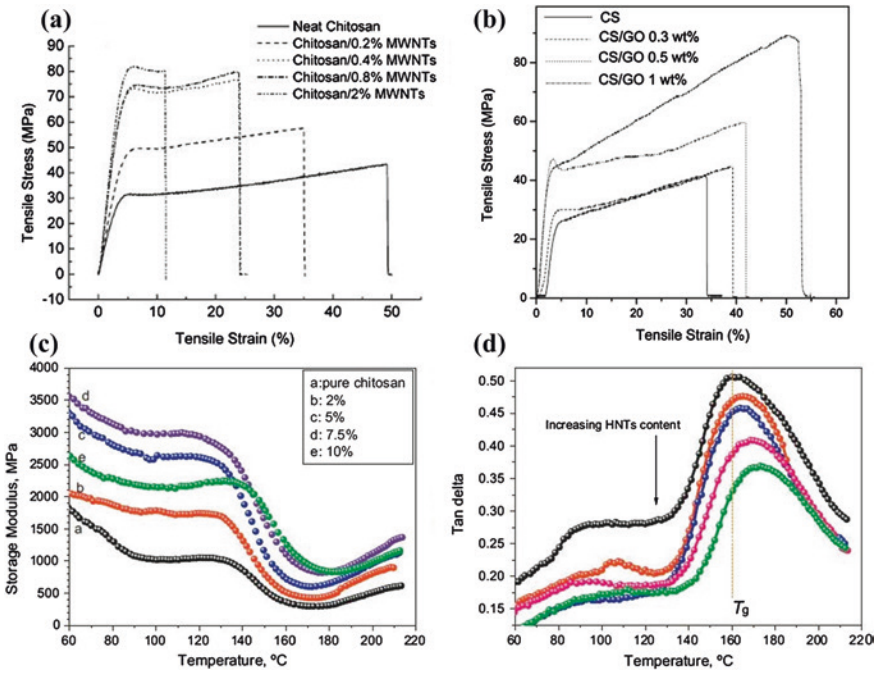

Fig. 5 **a** Typical stress–strain curves of neat chitosan and its MWNTs nanocomposite at a crosshead speed of 5 mm/min, [76] **b** Stress–strain behaviors for the films of CS/GO nanocomposites with different GO loadings [77]. Storage modulus (C) and tan δ (D) versus temperature curves for chitosan/HNTs nanocomposite films [83]

the increase in chitosan concentration whereas the elongation at break decreases [78]. Wang et al. found that hardness and elastic modulus were gradually enhanced with increase in clay concentration in chitosan/montmorillonite nanocomposites [66]. To improve the mechanical properties of chitosan films, chitin whisker is used as an additive [79]. The tensile strength is sharply increased and elongation at break has significantly reduced with the addition of chitin whiskers. It is observed that tensile strength increases exponentially until it reaches a threshold with the increase in whiskers content. Sepiolite (SP) has also been used as reinforce nanofiller to increase the mechanical strength of chitosan (CS)/poly (vinyl alcohol) (PVA) matrix [80]. Tensile strength and tensile modulus were enhanced after introducing the SP into the CS/PVA matrix. It is observed that mechanical properties increase up to certain limit of nanofiller addition. This behavior can be explained by the fact that there exist three-dimensional (3D) network formations through the hydrogen bonds between SP and PVA, PVA and CS. The tensile strength and elongation at break of nanocomposites decrease simultaneously with increasing the SP content. More CS was adhered to the surface of negatively charged SP due to the electrostatic attraction with the increment of SP content. These phenomena will weaken the interaction between CS and PVA, thus, the 3D

hydrogen bond network destroys partly. Destruction of the three-dimensional network may lead to the decrease of the mechanical properties of the nanocomposite. The chitin hydrogels are relatively weak which resists their application where high stress is required. Chitin/halloysite nanotubes (HNTs) hybrid hydrogels were prepared with different ration of chitin and HNTs to improve their mechanical property [81]. The Fracture stress of the chitin–HNTs hybrid hydrogels significantly increases in comparison to the pure chitin hydrogels. The mechanical performance is proportional to the content of HNTs in hybrid hydrogels. It is observed that the maximum compressive strength of HNTs hybrid hydrogel is ~300 % higher than pure chitin hydrogels. The chitin–HNTs hybrid hydrogels exhibit a significant increase in mechanical strength as compared to pure chitin and chitosan hydrogels due to the reinforcing effect of HNTs in chitin and the interfacial interactions. The rheological measurement shows that absolute values of the shear modulus (G′) for the chitin–HNTs hybrid hydrogels substantially increase with the loading of HNTs especially at high HNTs loadings which is in good agreement with the change of compressive mechanical properties. A significant synergistic effect of Fe_3O_4 and MWNT provides enhanced mechanical properties to chitosan. A 5 wt% loading of Fe_3O_4/MWNT in the nanocomposite enhances the tensile strength and tensile modulus [72]. Tensile strength of 5 % Fe_3O_4/MWNT/chitosan nanocomposite was 159 % higher than that of chitosan. The elastic modulus of the 5 % Fe_3O_4/MWNT/chitosan was 179 % higher than that of chitosan. Variations in storage modulus (E') and tan δ of the 5 % MWNT/chitosan and 5 % Fe_3O_4/MWNT/chitosan nanocomposites are significant. It was found that the 5 % Fe_3O_4/MWNT/chitosan nanocomposite had a higher E' than 5 % MWNT/chitosan nanocomposite which suggests that the interactions between chitosan, MWNT, and Fe_3O_4 are strong and allow an efficient load transfer. The glass transition temperature (T_g) of 5 % Fe_3O_4/MWNT/chitosan is lower than 5 % MWNT/chitosan, which are 161 and 166 °C, respectively. T_g has shifted to lower region and elastic modulus is higher, such type of behavior of Fe_3O_4 is known as antiplasticizing effect. Silva et al. reported that chitosan membrane with 5 (w/w%) halloysite nanotubes (HNTs) has the highest strength as compared to other concentration [73]. The higher strength of chitosan/HNTs is attributed to the interaction of HNTs with the chitosan. The hydroxyl groups on the edge and the surface of HNTs can interact with the hydroxyl and amino groups of the glucosamine rings of the chitosan. This interaction is important for facilitating the stress transfer (generated in the chitosan matrix) to the HNTs which act as a reinforcing agent. The unique synergistic effect of 2D nanotube (CNT) and 1D clay platelet on the reinforcing of chitosan has been demonstrated by Tang et al. [82]. It is observed that the increase of tensile strength is saturated at 3 wt% clay for chitosan/clay and 0.4 wt% CNTs for chitosan/CNTs compopsite which may be influenced by the aggregation of the nanofillers at higher content. The tensile strength and Young's modulus of the nanocomposites are significantly improved by about 171 and 124 %, respectively, as compared with neat chitosan with the incorporation of 3 wt% clay and 0.4 wt% CNTs. The dynamic modulus and tan δ spectra of pure chitosan and chitosan/HNTs nanocomposite films are compared in Fig. 5c, d.

[83]. The modulus of the chitosan/HNTs nanocomposite films increase with the increase in HNTs content until the loading of HNTs reaches at 7.5 %, due to the reinforcing effect of HNTs in chitosan. HNTs are known as inorganic rigid silicate nanotubes with high aspect ratio and hence interfacial reactions taking place between HNTs and chitosan, the chitosan/HNTs nanocomposite films show higher modulus both in glassy as well as rubbery state. Apart from the increased storage modulus, the glass transition temperature of chitosan also increases using HNTs. Composites with 10 wt% HNTs show the maximum T_g at 172 °C, which is 12 °C higher than that of pure chitosan.

7 Tissue Engineering

The cell adhesion, spreading, and cytoskeleton organization are the important parameters in evaluating the cellular compatibility and suitability of biomaterials for a required application. Singh et al. successfully combined the biocompatible nature of chitin with the high electrical conductivity of carbon nanotube to create a biocompatible, electrically conducting scaffold permissive for mesenchymal stem cell (MSCs) function [84]. They have used multiwall carbon nanotubes (MWNTs) coated with carboxymethyl cellulose to prepare composites films with varying weight fraction of MWCNTs. They have performed MTS assay to determine the growth rate and number of MSCs present on the chitin–MWNT films at various MWNT concentrations (Fig. 6a). The MSC viability on chitin–MWNT films was tested using the live/dead viability assay where green fluorescence indicates live cells and red fluorescence shows dead cells as shown in Fig. 6b. The viability of MSCs on chitin–MWNT composite scaffolds was checked by using live and dead assay upto 14 days. The composite film with 0.07 weight fraction of MWNT revealed an increased cell binding capacity. The poor binding of cell of 0.1 weight fraction compared to the 0.07 weight fraction is due to increased hydrophobicity with higher nanotube concentrations. Peter et al. developed chitin/bioactive glass ceramic nanoparticles (nBGC) composite scaffold macro porous in nature of pore size 150–500 μm for tissue engineering applications [85]. Cell culture studies were conducted with osteoblast cells like MG-63. Composites scaffold offers suitable environment to the cells for attachment to the wall of the scaffold composite. The nanocomposite scaffolds are biodegradable and biocompatible and can be used for tissue engineering applications. Gaharwar et al. prepared bio-nanocomposites by the addition of chitosan to silicate (laponite) cross-linked poly(ethelene oxide) (PEO) for creating improved scaffolds for bone repair [86]. The addition of chitosan retards the release of entrapped model macromolecular drug (albumin) from the bio-nanocomposites. The effect is prominent with higher concentration of chitosan and the burst release is suppressed and become sustained after 12 h. An increase in preosteoblast cells adhesion and spreading was observed with the increase in chitosan concentration in chitosan-containing silicate cross-linked PEO bio-nanocomposites. Jayakumar et al. have prepared chitin–chitosan/nano-TiO_2

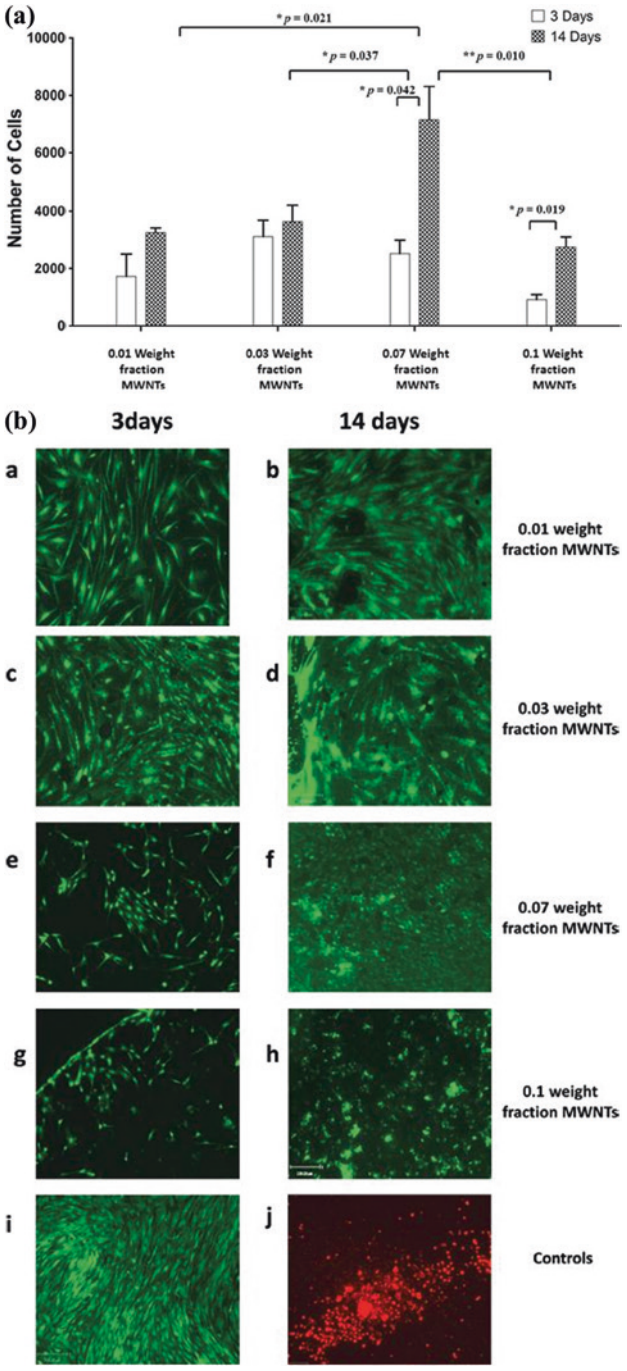
(a)
3 Days
14 Days
*p = 0.021
*p = 0.037
**p = 0.010
*p = 0.042
*p = 0.019
Number of Cells
10000
8000
6000
4000
2000
0
0.01 Weight fraction MWNTs
0.03 Weight fraction MWNTs
0.07 Weight fraction MWNTs
0.1 Weight fraction MWNTs
(b)
3days
14 days
a
b
0.01 weight fraction MWNTs
c
d
0.03 weight fraction MWNTs
e
f
0.07 weight fraction MWNTs
g
h
0.1 weight fraction MWNTs
i
j
Controls

Fig. 6 **a** MTS assay quantifying MSC proliferation on different concentrations of chitin–MWNT films. The positive control in this case is the tissue culture plate (plastic). A cell count below 250 was disregarded from the analysis due to the inherent limitation of the assay. Data are given as mean+standard error. **b** Live and dead viability assay to test the viability of MSCs on the chitin–MWNT film scaffolds. Cells were seeded on the scaffolds and were stained with the Live/Dead viability stain. *Green cells* showed the number of live cells and red cells showed dead cells due to the excitation of fluorescent dye (calcein AM) at 490 nm. The images were obtained after 3 d (*left column*) and 14 d (*right column*) of cells seeding [84]

composites scaffold for bone tissue engineering [75]. They have shown that the cell attachment increases significantly in nanocomposites scaffold as compared to control scaffold. Kumar et al. have prepared β-chitin hydrogel/nano-hydroxyapatite (nHAp) nanocomposites scaffolds with different concentration of nHAp [69]. They have found that more cells were found on the β-chitin composites scaffolds than that of β-chitin control scaffolds. Chen et al. have developed a novel chitosan–gold (CS–Au) hybrid hydrogel as a delivery system for anticancer drug, doxorubicin (DOX) [87]. Encapsulated model drug releases from the hydrogel in a sustained manner over 10 days and the drug releasing property is also affected by the external pH stimuli which showed its potential application for smart drug delivery. Kumar et al. have produced pectin–chitosan nanocomposites scaffold containing $CaCO_3$ nanopowder with an intention to use it in biomedical application such as tissue engineering and drug delivery [88]. The scaffolds have adequate potential for efficient cell adhesion, proliferation and also proved its potency in site-specific drug delivery. Nanocomposites scaffolds of chitin–chitosan with nano-ZrO_2 have been developed by Jayakumar et al. [89]. The nanocomposite scaffold increased the cell attachment significantly as compared to control scaffolds due to large surface area.

8 Drug Release

The drug release kinetics from nanocarriers depends on various factors such as pH, degaradation rate, particle size, and interaction between the drug and the surface of the polymer [90]. Ardeshirzadeh et al. have developed polyethylene oxide (PEO)/chitosan (CS)/graphene oxide (GO) electrospun nanofibrous scaffolds for controlled release of Doxorubicin (DOX) [91]. The different content of GO (0.1, 0.2, 0.5, and 0.7 wt%) was used to prepare the scaffolds. They have studied the DOX release from GO-DOX and PEO/CS/GO/DOX at a temperature of 37 °C in the phosphate buffer solutions (pH = 5.3 and 7.4) and is shown in Fig. 7a. DOX releases from GO-DOX and PEO/CS/GO/DOX nanofibers occurred at slower and controlled manner at pH 7.4 as compared to the release in acidic condition (pH 5.3). Hydrogen-bonded interaction between GO and DOX become stable in neutral condition which results in controlled release of DOX from GO/DOX and PEO/CS/GO/DOX. In acidic condition, such type of hydrogen-bonded interaction becomes weaker resulting faster release of drug. The diffusion of DOX from interconnected

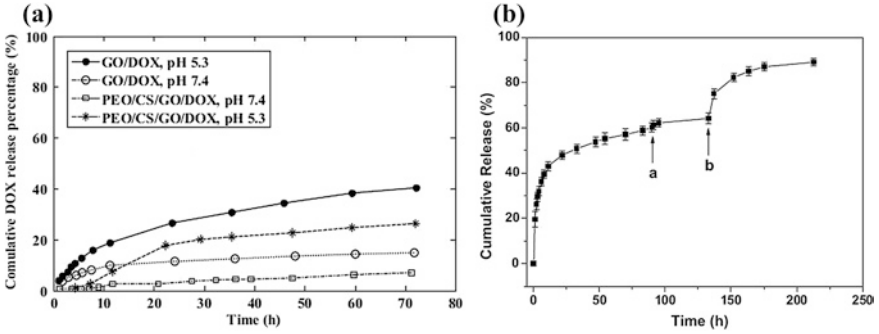

Fig. 7 **a** The DOX release profiles of GO-DOX and PEO/CS/GO/DOX at pH of 5.4 and 7.3. [91]. **b** Cumulative release of DOX·HCl from CS–Au hydrogel at 37 °C and pH 7.4. Point a: increase temperature to 70 °C for 1 h, then reincubate the hydrogel in PBS at 37 °C; Point b: the pH value of PBS was changed to 3.0 [87]

nanofibrous layer exerted an additional barrier for controlled and prolonged release rate. Such type of system could be a promising candidate for controlled and targeted delivery. Chen et al. studied the cumulative doxorubicin (DOX) release from chitosan–gold (CS–Au) hybrid hydrogel at 37 °C in PBS solution (Fig. 7b) [87]. CS–Au hydrogel shows sustained release profile with 60 % of the loaded DOX to the medium within 80 h. No more DOX release was found after that due to the stable gel network which retards the diffusion of DOX from the deep gel pores. Therefore, they have increased the incubation temperature to destroy the hydrogel structure to accelerate the release rate. After 30 h additional incubation at 70 °C cumulative release did not exceed 65 %. Chitosan is in the deprotonated state at pH 7.4 and it is negatively charged while DOX is positively charged. CS and DOX can form complex through the strong electrostatic interaction which is responsible for incomplete release of DOX from CS–Au hydrogel. A burst release was observed when the hydrogel was immersed in PBS with pH 3.0. More than 90 % of loaded DOX was released into the medium after 30 h of incubation at pH 3.0 which confirmed the electrostatic interaction between CS and DOX. The drug release profile is also influenced by external stimuli, such as temperature and pH. So CS–Au hydrogel may be used as a smart drug release system. Kumar et al. have shown the release of Fosamax from the pectin, chitin, and nano-$CaCO_3$ nanocomposite scaffolds [88]. Sustained release of drug was observed from the scaffold. Release rate can be correlated with the hydrophilic nature of Fosamax which will diffuse out in the aqueous medium easily. Nanohydrogel composed of chitosan and montmorillonite (MTT) was prepared for drug release behavior following electrostimulation by Liu et al. [92]. The drug release behavior was strongly influenced by the concentration of MTT under an applied voltage. Vitamin B_{12} displays pseudo-zero-order release kinetics and the release mechanism shifted from being diffusion-controlled to swelling-controlled mode with a low MMT content (1 wt%) but with an MMT content exceeding 1 wt%, both the diffusion exponent '*n*' and the

responsiveness to electrical stimulation were decreased. Nivethaa et al. synthesized chitosan/gold nanocomposite through simple chemical reduction method for drug delivery carrier for 5-fluorouracil [93]. The release of 5-fluorouracil shows two phase behavior; one up to 40 h and the next phase is up to 72 h. Slow, sustained, and prolonged release was observed in first phase and a sudden burst release was observed during the second phase. First phase release fitted well to the zero-order release kinetics which refers to the constant release of drug from a drug delivery device and the second phase release fitted well to the Higuchi kinetics.

9 Antimicrobial Activity

Shariatinia et al. have developed nanocomposite film of chitosan (CS)/phosphoramide (Ph)/silver nanoparicles (Ag NPs) containing 1–5 % of Ag NPs and investigated their antibacterial activity [94]. They have performed in vitro antibacterial activities of chitosan (CS), phosphoramide (Ph), Ag nanoparticle (Ag NPs), nanocomposite films containing 1–5 % Ag NPs and nanocomposite films of 1–5 % Ag NPs (as control films without Ph) using four different bacteria: two Gram-positive *Staphylococcus aureus*, *Bacillus cereus* and two Gram-negative *Escherichia coli*, *P. aeruginosa* bacteria. The results are summarized in Table 1. Tested samples are much more effective against gram-positive bacteria than that of gram-negative one because of lack of outer membrane in gram-positive bacteria. Antibacterial effect has increased by increasing the Ag NPs percent from 1 to 5 % in the CS/Ph/Ag Nps nanocomposite films (Fig. 8) comparing zone of inhibition (mm). The control films containing 1–5 % Ag NPs showed less antibacterial

Table 1 The inhibition zone (mm) measured for the antibacterial activities (Mean ($n = 3$) ± standard deviation) [94]

Sample	Bacterium type			
	S. aureus	*B. cereus*	*E. coli*	*P. aeruginos*
Ag NPs	10 ± 0.46	8.8 ± 0.47	7.5 ± 0.50	7.66 ± 0.48
Phosphoramide (Ph)	7.5 ± 0.45	7.2 ± 0.48	6.9 ± 0.48	6.7 ± 0.46
Chitosan (CS)	13.33 ± 0.50	11.66 ± 0.49	9.66 ± 0.49	10.33 ± 0.47
CS+Ph	14.66 ± 0.49	12.66 ± 0.48	10 ± 0.47	11 ± 0.49
CS+AgNPs 1 %	15.50 ± 0.47	13.50 ± 0.50	11.33 ± 0.48	13 ± 0.50
CS+Ag NPs 2 %	15.55 ± 0.48	13.80 ± 0.46	11.50 ± 0.50	13.10 ± 0.48
CS+Ag NPs 3 %	16 ± 0.50	14 ± 0.48	11.66 ± 0.47	13.33 ± 0.49
CS+Ag NPs 4 %	16.33 ± 0.46	14.33 ± 0.49	11.80 ± 0.49	13.50 ± 0.50
CS+AgNPs 5 %	16.66 ± 0.48	14.50 ± 0.50	12 ± 0.48	13.66 ± 0.47
Film 1	16 ± 0.46	14 ± 0.47	11.80 ± 0.50	13.33 ± 0.46
Film 2	16.66 ± 0.47	14.50 ± 0.50	12 ± 0.45	13.50 ± 0.50
Film 3	17.33 ± 0.49	14.80 ± 0.49	12.33 ± 0.48	13.66 ± 0.48
Film 4	17.66 ± 0.48	15 ± 0.48	12.50 ± 0.49	13.70 ± 0.47
Film 5	18.66 ± 0.47	15.66 ± 0.46	12.66 ± 0.48	13.80 ± 0.49

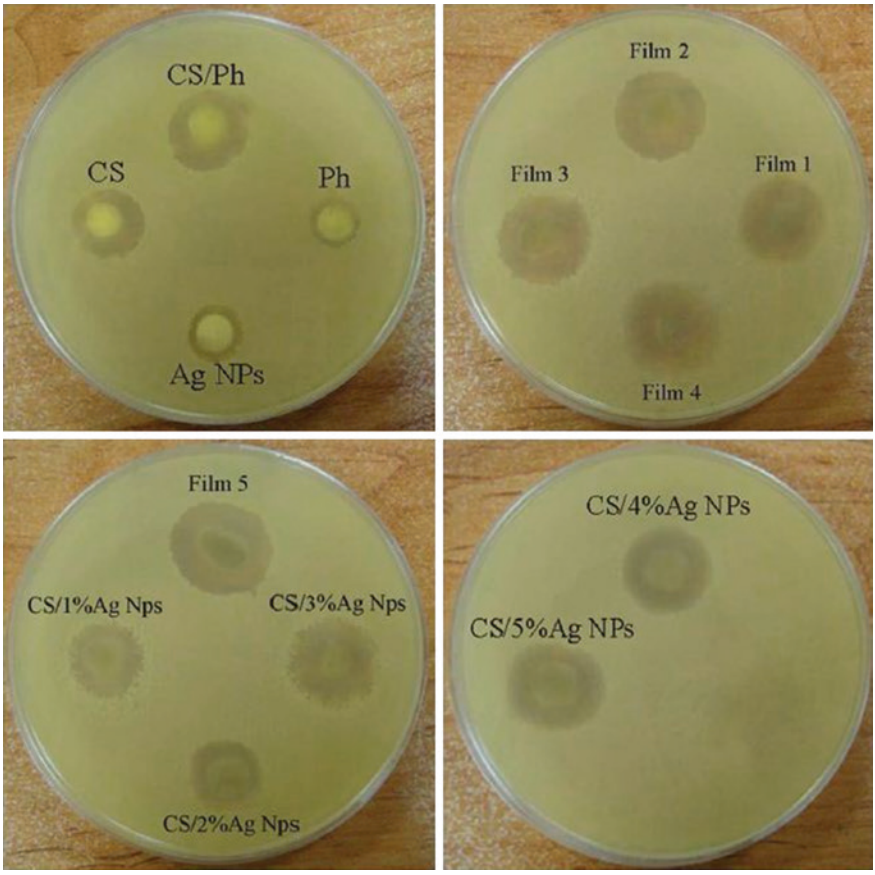

Fig. 8 The digital photographs of antibacterial activities of Ag NPs, chitosan (CS), phosphoramide (Ph), and CS/Ph film, nanocomposite films 1–5 plus CS/1–5 % Ag Nps against *S. aureus* bacterium [94]

activities than those nanocomposoites films. Sharma et al. have prepared silver nanocomposite film using chitosan and alginate (1:1) blend and tested their antibacterial activity against gram-positive and gram-negative bacteria [95]. The blended nanocomposite film showed antibacterial activity against both gram-negative and gram-positive bacteria with more inhibition using gram-positive bacteria. Usually gram-positive bacteria have less negative charge on its cell wall as compared to gram-negative bacteria. The silver nanocomposites have shown overall negative charge which will interact more with the gram-positive bacteria as compared to higher negative charge containing gram-negative bacteria. Hebeish et al. prepared chitosan-grafted-poly acrylonitrile silver nanocomposites (CS-g-PAN/Ag) and performed antibacterial test using *E. coli* and *S. aureus* [61]. The growth of the bacteria was significantly affected in CS-g-PAN/Ag nanocomposite than that of PAN and

CS-g-PAN copolymer. Silver nanocomposites of poly(ethylene glycol-di-aldehyde) cross-linked chitosan have shown good antibacterial activity toward *E. coli* [96]. Regiel-Futyra et al. checked antibacterial activity of chitosan–gold nanocomposite where chitosan of different molecular weight and different degree of deacetylation was used to prepare nanocomposite [60]. Nanocomposite based on chitosan with medium molecular weight with highest gold content had very good antibacterial effect in comparison to chitosan with low and high molecular weight CS-based composites. Chitosan/ZnO nanocomposite films exhibit good antibacterial activity against gram-positive and gram-negative bacteria [97]. Han et al. have performed antibacterial test of pure chitosan and montmorillonite and chitosan–montmorillonite nanocomposites [70]. Interestingly, chitosan–montmorillonite nanocomposites show higher antimicrobial activity than pure chitosan. Chitosan itself shows antibacterial activity due its cationic nature. Cationic charge of chitosan is neutralized via an electrostatic interaction with anionic silicate layer. Hence, the enhanced antimicrobial activity of nanocomposites is due to synergic effect because the chitosan

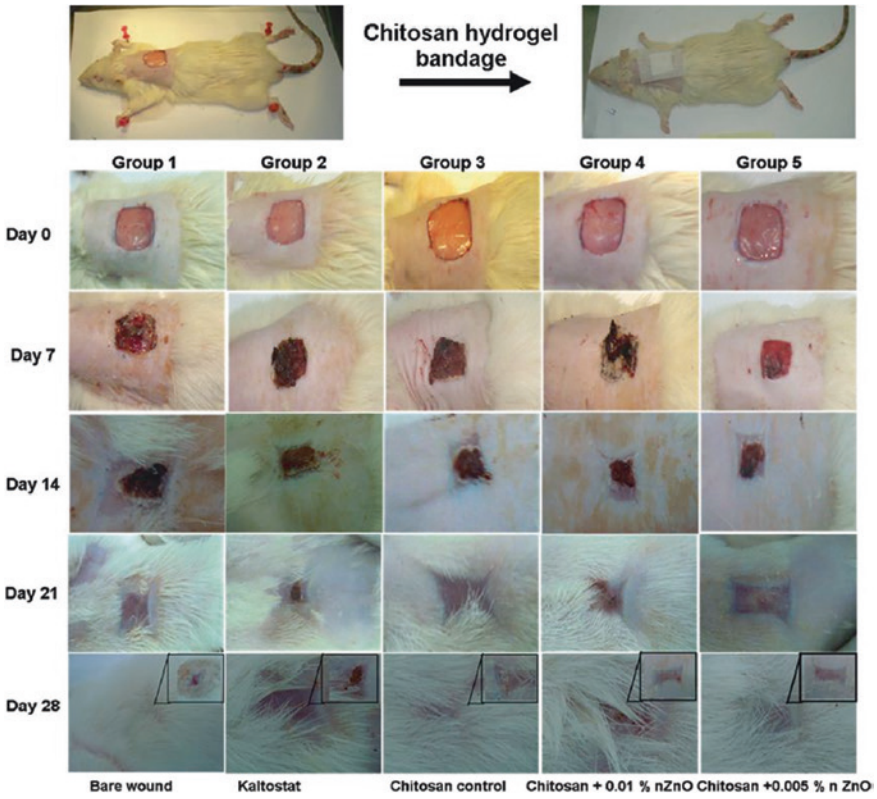

Fig. 9 Photographs of an in vivo wound healing study. Note the extent of wound closure in the wounds treated with chitosan control and CZBs [100]

molecules are evenly distributed through the inorganic matrix. Nanocomposite films of chitosan, starch, glycerin, cyclophosphamide, and Fe_3O_4 nanoparticles have shown good antibacterial activity against gram-positive bacteria as compared to gram-negative one [98]. Wysokowski et al. have shown that β-chitin/ZnO nanocomposite scaffolds exhibit good antibacterial activity against gram-positive Bacillus subtilis but there is no effect on gram-negative *E. coli* [99].

10 Implant Materials

Chitosan nanocomposites are widely used as implant materials. Sudheesh Kumar et al. developed chitosan hydrogel/nano-ZnO nanocomposite bandages (CZBs) via the incorporation of ZnO nanoparticle (nZnO) into chitosan hydrogel [100]. In vivo study was conducted in Sprague-Dawley (SD) rats to prove the enhanced wound healing ability of the prepared CZBs. Figure 9 shows the digital photographs of an in vivo wound healing study. Chitosan control as well as nanocomposites bandages show excellent healing after 1 and 2 weeks, compared to Kaltostat and bare wound. Wounds treated with chitosan control and CZBs achieved significant closure to ~90 % after 2 weeks as compared to Kaltostat-treated wound and bare wounds, which showed 70 % closure (Fig. 10a). There

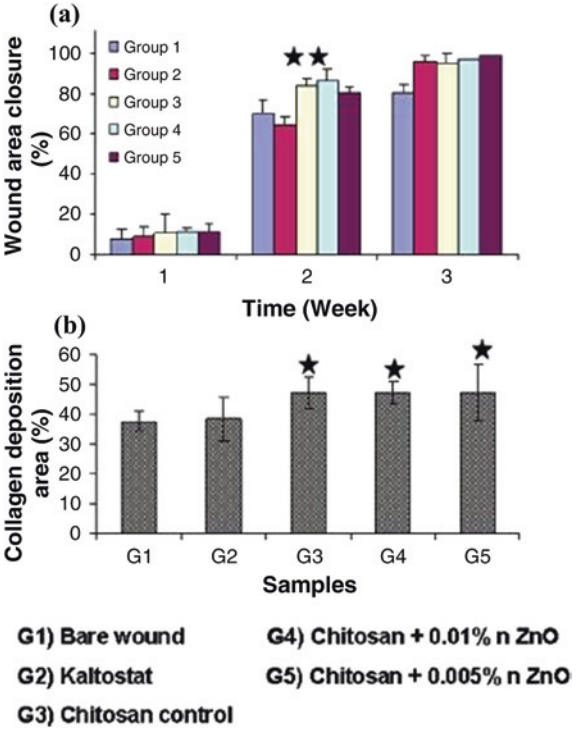

Fig. 10 **a** Evaluation of the wound area closure and **b** study of the collagen deposition area. (In both graphs, the *star symbols* represent the p 0.05 level, indicating that the means are significantly different, compared with the control) [100]

was enhanced collagen deposition in the wound healing assisted by the chitosan controls and CZBs after 4 weeks. CZBs showed controlled degradation, enhanced blood clotting, excellent platelet activation ability, cytocompatibility, and antibacterial activity. All these properties indicate that advanced CZBs can be used for burn, chronic, and diabetic wound infections. The development of a CS–hyaluronan/nano-chondroitin sulfate ternary composite sponge for medical use has been reported by Anisha et al. This nanocomposite sponges with enhanced swelling and blood clotting ability were cytocompatible and showed enhanced proliferation of human dermal fibroblast cells [101]. Nano-Ag incorporated chitosan films were developed which showed faster wound healing in Spraque Dawley rats [102].

Acknowledgments The author (A K. Mahanta) gratefully acknowledges the financial support from Council for Scientific and Industrial Research (CSIR-UGC), New Delhi in the form of fellowship. The authors also acknowledge the receipt of research funding from Council for Scientific and Industrial Research (CSIR), New Delhi, Government of India (Project No. 02(0074)/12/EMR-II).

References

1. Vacanti JP, Vacanti CA, Lanz RP, Langer R, Vacanti J (2000) Principles of tissue—engineering, 2nd edn. Academic Press, California 3
2. Hench LL, Polak JM (2002) Third-generation biomedical materials. Science 295:1014–1017
3. Ramires PA, Romito A, Cosentino F, Milella E (2001) The influence of titania/hydroxyapatite composite coatings on in vitro osteoblasts behavior. Biomaterials 22:1467–1474
4. Rinaudo M (2006) Chitin and chitosan: properties and applications. Prog Polym Sci 31:603–632
5. Aranaz I, Mengíbar M, Harris R, Panos I, Miralles B, Acosta N, Galed G, Heras A (2009) Functional characterization of chitosan. Curr Chem 3:203–230
6. Honarkar H, Barikani M, Honarkar H, Barikani M (2009) Applications of biopolymers I: Chitosan. Monatsh Chem 140:1403–1420
7. Hein S, Wang K, Stevens WF, Kjems J (2008) Chitosan composites for biomedical applications: status, challenges and perspectives. Mater Sci Technol 24:1053–1061
8. Shi C, Zhu Y, Ran X, Wang M, Su Y, Cheng T (2006) Therapeutic potential of chitosan and its derivatives in regenerative medicine. J Surg Res 133:185–192
9. Dash M, Chiellini F, Ottenbrite RM, Chiellini E (2011) Chitosan a versatile semi-synthetic polymer in biomedical applications. Prog Polym Sci 36:981–1014
10. Rudall K, Kenchington MW (1973) The chitin system. Biol Rev 48:597–633
11. Ifuku S, Morooka S, Morimoto M, Saimoto H (2010) Acetylation of chitin Nanofibers and their transparent nanocomposite films. Biomacromolecules 11:1326–1330
12. Onishi H, Machida Y (1999) Biodegradation and distribution of water-soluble Chitosan in mice. Biomaterials 20:175–182
13. Ravi Kumar MNV, Muzzarelli RAA, Muzzareli C, Sasfiwa H, Domb AJ (2004) Chitosan chemistry and pharmaceutical perspectives. Chem Rev 104:6017–6084
14. Honarkar H, Barikani M, Honarkar H, Barikani M (2009) Applications of biopolymers I: Chitosan. Monatsh Chem 140:1403–1420
15. Chitin Tasch P (1979) In: Fairbridge RW, Jablonski D (eds) Paleontology, encyclopedia of earth science. Springer, Berlin, pp 186–189
16. Jang MK, Kong G, Jeong Y, Lee CH, Nah JW (2004) Physicochemical characterization of α chitin, β chitin, and γ chitin separated from natural resources. J Polym Sci part A: PolymChem 42:3423–3432

17. Anitha A, Sowmya S, Sudheesh Kumar PT, Deepthi S, Chennazhi KP, Ehrlirch H, Tsurkan M, Jayakumar R (2014) Chitin and chitosan in selected biomedical applications. Prog Polym Sci 39:1644–1667
18. Gong X, Peng S, Wen W, Sheng P, Li W (2009) Design and fabrication of magnetically functionalized core/shell microspheres for smart drug delivery. Adv Funct Mater 19:292–297
19. Hsieha WC, Changb CP, Gaoc YL (2006) Controlled release properties of Chitosan encapsulated volatile Citronella Oil microcapsules by thermal treatments. Colloids Surf B 53:209–214
20. Yamamoto H, Amaike M (1997) Biodegradation of cross-linked chitosan gels by microorganisms. Macromolecules 30:3936–3937
21. Risbud MV, Bhonde RR (2000) Polyacrylamide-chitosan hydrogels: in vitro biocompatibility and sustained antibiotic release studies. Drug Deliv 7:69–75
22. Roughley P, Hoemann C, Desrosiers E, Mwale F, Antoniou J, Alini M (2006) The potential of chitosan-based gels containing invertebraldisc cells for nucleus pulposus supplementation. Biomaterials 27:388–396
23. Ehrlich H, Krajewska B, Hanke T, Born R, Heinemann S, KniebC Worch H (2006) Chitosan membrane as a template for hydroxyap-atite crystal growth in a model dual membrane diffusion system. J Membr Sci 273:124–128
24. Jayakumar R, Divya RVV, Shalumon KT, Sudheesh Kumar PT, Nair SV, Furuike T, Tamura H (2009) Bioactive and osteoblast cell attachmentstudies of novel α- and β- chitin membranes for tissue-engineering applications. Int J Biol Macromol 45:260–264
25. Jayakumar R, Prabaharan M, Nair SV, Tamura H (2010) Novel chitin and chitosan nanofibers in biomedical applications. Biotechnol Adv 28:142–150
26. Morganti P, Morganti G (2008) Chitin nanofibrils for advanced cosmeceuticals. Clin Dermatol 26:334–340
27. Jayakumar R, Reis RL, Mano JF (2007) Synthesis and characterization of pH-sensitive thiol-containing chitosan beads for controlled drugdelivery applications. Drug Deliv 14:9–17
28. Prabaharan M, Mano JF (2005) Chitosan-based particles as controlled drug delivery systems. Drug Deliv 12:41–57
29. Anitha A, Divya RVV, Krishna R, Sreeja V, Selvamurugan N, Nair SV, Tamura H, Jayakumar R (2009) Synthesis, characterization, cyto-toxicity and antibacterial studies of chitosan, O-carboxymethyl, N, O-carboxymethyl chitosan nanoparticles. Carbohydr Polym 78:672–677
30. Anitha A, Deepagan VG, Divya RVV, Deepthy M, Nair SV, Jayakumar R (2011) Preparation, characterization, in vitro drug release and biologicalstudies of curcumin loaded dextran sulphate-chitosan nanoparti-cles. Carbohydr Polym 84:1158–1164
31. Drury JL, Mooney DJ (2003) Hydrogels for tissue engineering: scaffold design variables and applications. Biomaterials 24:4337–4351
32. Jayakumar R, Prabaharan M, Sudheesh Kumar PT, Nair SV, Tamura H (2011) Biomaterials based on chitin and chitosan in wound dressing applications. Biotechnol Adv 29:322–337
33. Prabaharan M, Jayakumar R, Nair SV (2012) Electrospun nanofibrous scaffolds -current status and prospects in drug delivery. Adv Polym Sci 246:241–262
34. Muramatsu K, Masuda S, Yoshihara S, Fujisawa A (2003) In vitro degra-dation behavior of freeze-dried carboxymethyl-chitin sponges processed by vacuum-heating and gamma irradiation. Polym Degrad Stab 81:327–332
35. Vacanti CA (2006) The history of tissue engineering. J Cell Mol Med 10:569–576
36. Krajewska B (2005) Membrane-based processes performed with use of chitin/chitosan materials. Sep Purif Technol 41:305–312
37. Venkatesan J, Kim SK (2010) Chitosan composites for bone tissue engineering—an overview. Mar Drugs 8:2252–2266
38. Jayakumar R, Nwe N, Tokura S, Tamura H (2007) Sulfated chitin and chi-tosan as novel biomaterials. Int J Biol Macromol 40:175–181

39. Tigli RS, Gumusderelioglu M (2009) Evaluation of alginate-chitosan semi IPNs as cartilage scaffolds. J Mater Sci Mater Med 20:699–709
40. Ragetly GR, Slavik GJ, Cunningham BT, Schaeffer DJ, Griffon DJ (2010) Cartilage tissue engineering on fibrous chitosan scaffolds produced by a replica molding technique. J Biomed Mater Res, Part A 93:46–55
41. Ragetly GR, Griffon DJ, Lee HB, Fredericks LP, Gordon-Evans W, Chung YS (2010) Effect of chitosan scaffold microstructure on mesenchymal stem cells chondrogenesis. Acta Biomater 6:1430–1436
42. Mourya VK, Inamdar NN (2008) Chitosan-modifications and applications: opportunities galore. React Funct Polym 68:1013–1051
43. Suh JKF, Matthew HWT (2000) Application of chitosan-based polysaccharide biomaterials in cartilage tissue engineering: a review. Biomaterials 21:2589–2598
44. Muzzarelli RAA (2009) Chitins and chitosans for the repair of wounded skin, nerve, cartilage and bone. Carbohydr Polym 76:167–182
45. Dai M, Zheng XL, Xu X, Kong XY, Li XY, Guo G, Luo F, Zhao X, Wei YQ, Qian Z (2009) Chitosan–alginate sponge: preparation and application in curcumin delivery for dermal wound healing in rat. J Biomed Biotechnol 595126/1–8
46. Sudheesh Kumar PT, Abhilash S, Manzoor K, Nair SV, Tamura H, Jayakumar R (2010) Preparation and characterization of novel β-chitin/nano silver composite scaffolds for wound dressing applications. Carbohydr Polym 80:761–777
47. Kofuji K, Huang Y, Tsubaki K, Kokido F, Nishikaw K, Isobe T, Murata M (2010) Preparation and evaluation of a novel wound dressing sheet comprised of β-glucan-chitosan complex. React Funct Polym 70:784–789
48. Cai ZX, Mo XM, Zhang KH, Fan LP, Yin AL, He CL, Wang HS (2010) Fabrication of chitosan/silk fibroin composite nanofibers for wound-dressing applications. Int J Mol Sci 11:3529–3539
49. Kang YO, Yoon IS, Lee SY, Kim DD, Lee SJ, Park WH, Hudson SM (2010) Chitosan coated poly (vinyl alcohol) nanofibers for wound dressings. J Biomed Mater Res B 92:568–576
50. Dong Y, Liu HZ, Xu L, Li G, Ma ZN, Han F, Yao HM, Sun YH, Li SM (2010) A novel CHS/ALG bi-layer composite membrane with sustained antimicrobial efficacy used as wound dressing. Chin Chem Lett 21:1011–1014
51. Radhakumary C, Antonty M, Sreenivasan K (2011) Drug loaded thermo responsive and cytocompatible chitosan based hydrogel as a potential wound dressing. Carbohydr Polym 83:705–713
52. Dev A, Binulal NS, Anitha A, Nair SV, Furuike T, Tamura H, Jayakumar R (2010) Preparation of novel poly (lactic acid)/chitosan nanoparticles for anti HIV drug delivery applications. Carbohydr Polym 80:833–838
53. Dev A, Mohan JC, Sreeja V, Tamura H, Patzke GR, Hussain F, Weyeneth S, Nair SV, Jayakumar R (2010) Novel carboxymethyl chitin nanoparticles for cancer drug delivery applications. Carbohydr Polym 79:1073–1079
54. Ravi Kumar MNV (2000) A review of chitin and chitosan applications. React Funct Polym 46:1–27
55. Sashiwa H, Aiba S (2004) Chemically modified chitin and chitosan as bio-materials. Prog Polym Sci 29:887–888
56. Ravi Kumar MNV, Muzzarelli RAA, Muzzarelli C, Sashiwa H, Domb AJ (2004) Chitosan chemistry and pharmaceutical perspectives. Chem Rev 104:6017
57. Yi H, Wu LQ, Bentley WE, Ghodssi R, Rubloff GW, Culver JN, Payne GF (2005) Biofabrication with chitosan. Biomacromolecules 6:2881–2894
58. Goldstein AS, Juarez TM, Helmke CD, Gustin MC, Mikos AG (2001) Effect of convection on osteoblastic cell growth and function in biodegradable polymer foam scaffolds. Biomaterials 22:1279–1288
59. Dutta PK, Srivastava R, Dutta J (2013) Functionalized nanoparticles and chitosan-based functional nanomaterials. Adv Polym Sci 254:1–50

60. Regiel-Futyra A, Lisḱiewicz MK, Sebastian V, Irusta Silvia, Arruebo M, Stochel G, Kyzioł A (2015) Development of noncytotoxic chitosan−gold nanocomposites as efficient antibacterial materials. Appl Mater Interf 7:1087–1099
61. Hebeisha AA, Ramadana MA, Montasera AS, Farag AM (2014) Preparation, characterization and antibacterial activity ofchitosan-g-poly acrylonitrile/silver nanocomposite. Int J Biol Macromol 68:178–184
62. Naseri N, Algan C, Jacobs V, John M, Kristiin Oksman K, Mathew AP (2014) Electrospun chitosan-based nanocomposite mats reinforced withchitin nanocrystals for wound dressing. Carbohydr Polym 109:7–15
63. Liu M, Wu C, Jiao Y, Xiong S, Zhou C (2013) Chitosan–halloysite nanotubes nanocomposite scaffolds for tissue engineering. J Mater Chem B 1:2078–2089
64. Duan B, Liu F, He M, Zhang L (2014) Ag–Fe_3O_4 nanocomposites@chitin microspheres constructed by in situ one-pot synthesis for rapid hydrogenation catalysis. Green Chem 16:2835–2845
65. Huang H, Yuan Q, Yang X (2005) Morphology study of gold–chitosan nanocomposites. J Colloid Interf Sci 282:26–31
66. Wang SF, Shen L, Tong YJ, Chen L, Phang IY, Lim PQ, Liu TX (2005) Biopolymer chitosan/montmorillonite nanocomposites: preparation and characterization. Polym Degrad Stab 90:123–131
67. Darder M, Colilla M, Hitzky R (2003) Biopolymer—clay nanocomposites based on chitosan intercalated in montmorillonite. Chem Mater 15:3774–3780
68. Liu M, Zhang Y, Li J, Zhou C (2013) Chitin-natural clay nanotubes hybrid hydrogel. Int J Bio Macromol 58:23–30
69. Sudheesh Kumar PT, Srinivasan S, Lakshmanan VK, Tamura H, Nair SV, Jayakumar R (2011) b-Chitn hydrogel/nanohydroxyapatite composite scaffolds for tisuue engineering applications. Carbohydr Polym 85:584–591
70. Han YS, Lee SH, Choi KH, Park I (2010) Preparation and characterization of chitosan-clay nanocomposites with antimicrobial activity. J Phys Chem Solids 71:464–467
71. Anisha BS, Sankar D, Mohandas A, Chennazhi Nair, Jayakumar R (2013) chitosanohyaluronan/nano chondroitin sulfate ternary composite sponges for medical use. Carbohydr Polym 92:1470–1476
72. Marroquin JB, Rhee KY, Park SJ (2013) Chitosan nanocomposite films: Enhanced electrical Conductivity, thermal stability, and mechanical properties. Carbohydr Polym 92:1783–1791
73. Silva RTD, Pasbakhsh P, Goh KL, Chai SP, Ismail H (2013) Physico-chemical characterization of chitosan/halloysite composite membranes. Polym Test 32:265–271
74. Azizi S, Ahmad MB, Ibrahim NA, Hussein MZ, Namvar F (2014) Preparation and properties of poly (vinyl alcohol)/chitosan Blend Bio-nanocomposites reinforced by cellulose nanocrystals. Chin J Polym Sci 12:1620–1627
75. Jayakumar R, Ramachandran R, Divyarani VV, Chennazhi KP, Tamura H, Nair SV (2011) Fabrication of chitin-chitosan/nano TiO_2-composite scaffolds for tissue engineering application applios. Int J Biol Macromol 48:336–344
76. Wang SF, Shen Lu, Zhang WD, Tong YJ (2005) Preparation and mechanical properties of chitosan/carbon nanotubes composites. Biomacromolecules 6:3067–3072
77. Yang X, Tu Y, Li L, Shang S, Tao X (2010) Well-disperesed chitosan/graphene oxide nanocomposites. Appl Mater Interf 6:1707–1713
78. Casariego A, Souza BWS, Cerqueira MA, Teixeira JA, Cruz L, Diaz R, Vicente AA (2009) Chitosan/clay films properties as affected by biopolymer and clay micro/nanoparticles' concentrations. Food Hydrocoll 23:1895–1902
79. Rubentheren V, Ward TA, Chee CY, Tang CK (2015) Processing and analysis of chitosan nanocomposites reinforced with chitin whiskers and tannic acid as a crosslinker. Carbohydr Polym 115:379–387
80. Huang D, Mu B, Wang A (2012) Preparation and properties of chitosan/poly (vinyl alcohol) nanocomposite film rein forced with rod-like sepiolite. Mater Lett 86:69–72

81. Liu M, Zhang Y, Li J, Zhou C (2013) Chitin-natural clay nanotubes hybrid hydrogel. Int J Biol Macromol 58:23–30
82. Tang C, Xiang L, Su J, Wang K, Yang C, Zhang Q, Fu Q (2008) Largely improved tensile properties of chitosan film via unique synergistic reinforcing effect of carbon nanotube and clay. J Phys Chem B 112:3876–3881
83. Liu M, Zhang Y, Wu C, Xiong S, Zhou C (2012) Chitosan/halloysite nanotubes bionanocomposite: structure, mechanical properties and biocompatibility. Int J Biol Macromol 51:566–575
84. Singh N, Koziol KKK, Chen J, Patil AJ, Gilman JW, Trulove PC, Kafienah W, Rahatekar SS (2013) Iionic liquids-based processing of electrically conducting chitin nanocomposite scaffolds for stem cell growth. Green Chem 15:1192–1202
85. Peter M, Sudheesh Kumar PT, Binulal NS, Nair SV, Tamura H (2009) Development of novel a-chitin/nanobioactive glass ceramic composite scaffolds for tissue engineering applications. Carbohydr Polym 78:926–931
86. Gaharwar AK, Schexnailder PJ, Jin Q, Wu CJ, Schmidt G (2010) Addition of chitosan to silicate cross-linked PEO for tuning osteoblast cell adhesion and mineralization. Appl Mater Interf 2:3119–3127
87. Chen R, Chen Q, Huo D, Ding Y, Hu Y, Jiang X (2012) In situ formation of chitosan-gold hybrid hydrogel and its application for drug delivery. Colloids Surf B 97:132–137
88. Sudheesh Kumar PT, Ramya C, Jayakumar R, Nair SV, Lakshmanan (2013) Drug delivery and tissue engineering applications of biocompatible pectin-chitin/nano $CaCO_3$ composite scaffolds. Colloids Surf B 106:109–116
89. Jayakumar R, Ramachandran R, Sudheesh Kumar PT, Divyarani VV, Srinivasan, Chennazhi KP, Tamura H, Nair SV (2011) Fabrication of chitin-chitosan/nano ZrO_2 composite scaffolds for tissue engineering applications. Int J Biol Macromol 49:274–280
90. Zhang JL, Misra RDK (2007) Magnetic drug-targeting carrier encapsulated with thermosensitive smart polymer: core–shell nanoparticle carrier and drug release response. Acta Biomater 3:838–850
91. Ardeshirzadesh B, Anaraki NA, Irani M, Rad LR, Shamshiri S (2015) Controlled release of doxorubicine from electrospun PEO/chitosan/grapheme oxide nanocomposite nanofiberous scaffolds. Mat Sci Eng C 48:384–390
92. Liu KH, Liu TY, Chen SY, Liu DM (2008) Drug release behavior of chitosan—montmorillonite nanocomposite hydrogels following electrostimulation. Acta Biomater 4:1038–1045
93. Nivethaa EAK, Dhanavel S, Narayanan V, Vasu CA, Stephen (2015) An in vitro cytotoxicity study of 5-fluorouracil encapsulated shitosan/gold nanocomposites towards MCF-7 cells. RSC Adv 5:1024–1032
94. Shariatinia Z, Nikfar Z, Gholivand K, Tarei SA (2015) Antibacterial activities of novel nanocomposite biofilms of chitosan/phosphoramide/Ag NPs. Polym Compos 454–466
95. Sharma S, Sanpui P, Chattopadhyay A, Ghosh SS (2012) fabrications of antibacterial silver nanoparticle-sodium alginate-chitosan composite films. RSC Adv 2:5837–5843
96. Rao KSV, Reddy PR, Lee YI, Kim C (2012) Synthesis and characterization of chitosan-PEG-Ag nancomposites for antimicrobial application. Carbohydr Polym 87:920–925
97. Youssef AM, Yousef HA, Sayed SME, Kamel S (2015) Mechanical and antibacterial properties of novel high performance chitosan/nanocomposite films. Int J Biol Macromol 76:25–32
98. Shariatinia Z, Fazli M (2015) Mechanical properties and antibacterial activities of novel nanobiocomposite films of chitosan and starch. Food Hydrocoll 46:112–124
99. Wysokowski M, Motylenko M, Stocker H, Bazhenov VV, Langer E, Dobrowolska A, Czaczyk K, Galli R, Stelling AL, Behm T, Klapiszewski L, Ambrozewicz D, Nowacka M, Molodtsov SL, Abendroth B, Meyer DC, Kurzydlowski KJ, Jesionowski T, Ehrlich H (2013) An extreme of biomemitic approach: hydrothermal synthesis of b-chitin/ZnO nanostrustured composites. J Mater Chem B 1:6469–6476

100. Sudheesh Kumar PT, Lakshmanan VK, Anilkumar TV, Ramya C, Reshmi P, Unnikrishnan AG, Nair SV, Jayakumar R (2012) Flexible and microporus chitosan hydrogel/nano ZnO composite bandages for wound dressing. in vitro and in vivo evaluation. Appl Mater Interf 4:2618–2629
101. Anisha BS, Deepthi S, Annapoorna M, Chennazhi KP, Nair SV, Jayakumar R (2013) Chitosan–hyaluronan/nano chondroitin sulfateternary composite sponges for medical use. Carbohydr Polym 92:1470–1476
102. Lu S, Gao W, Gu HY (2008) Construction, application and biosafety of silve nanocrystalline chitosan wound dressing. Burns 34:623–628